VALIDATION OF FLUID-STRUCTURE COUPLING COMPUTATIONS FOR SOLID PROPELLANT ROCKET MOTORS APPLICATIONS

S. Cerqueira[*], *G. Chaineray*[‡], *B. Courbet*[‡], *M. Errera*[‡], *F. Feyel*[‡], *and F. Vuillot*[‡]
[*]CNES/DLA, Rond Point de l'Espace, 91003 Evry, France
[‡]ONERA, 29 avenue de la Division Leclerc, 92322 Chatillon, France

Abstract

A number of interacting phenomena, for instance Fluid-Structure Interaction (FSI), are of major importance for a wide range of applications. Fluid structure interactions have been shown to be extremely important while studying pressure oscillations in segmented solid rocket motors. This paper addresses the partitioned FSI procedure developed at ONERA between the two solvers CEDRE and ZeBuLoN for respectively flow and structure subsystems, with a particular emphasis on code coupling validation. Application to the field of solid rocket propulsion is investigated by simulating the VALDO-ONERA experimental device which is a cold flow experimental model for Solid Propellant Rocket Motors.

1. INTRODUCTION

Fluid-Structure Interaction (FSI) phenomena arises in many scientific and engineering applications including unsteady motions in Solid Propellant Rockets Motors (SPRM). To improve the physical understanding on pressure oscillations inside SPRM, ONERA has developed a coupling methodology involving two solvers, CEDRE and ZeBuLoN, for respectively flow and structure subsystems.

1.1 CEDRE : physical models and numerical methods

CEDRE is a software package whose key element is a code for numerical simulation in the field of energetics, with particular emphasis on propulsion applications. The code can handle several coupled physical subsystems, each of them being taken into account by a specialized time dependent solver :

- The compressible flow module solves the Navier-Stokes equations with any number of species and various possible models for chemical reactions. Turbulence is taken into account either in the RANS approach or through LES simulation [3]. In some cases, the fluid carries a liquid or solid disperse phase which can be simulated with a lagrangian or an eulerian approach.

- Heat transfer in solid walls is simulated by a conduction solver coupled with the fluid and radiation is available through a specific module.

- Several solvers under developpement will extend the simulation capacities for plasmas, liquid films ...

Moreover, for simulation domains not included in the package such as aeroelasticity or solid mechanics for instance, external coupling with other softwares is available.

The CEDRE code use a non-structured general mesh in which elements are polyhedrons with any number of faces (each internal face being connected with two cells). Solvers for conservation equations are based on a *cell-centered finite volume methodology*. Stable and precise evaluation of convective fluxes is obtained through a non-structured extension of MUSCL reconstruction techniques : in each cell, state variables

are supposed to be linear (or polynomial), gradients (and possibly higher order space derivatives) being evaluated through algebraic interpolation from a given stencil. This piecewise reconstruction, together with a nonlinear limitation procedure, allows two evaluations of state variables at each quadrature point along the interface between two cells, which are the input of an upwind numerical flux formula.

With the above space discretization techniques, balance equations are approximated as an ordinary differential equations system whose unknowns are the mean values of the conserved quantities on the mesh cells. Several options are available for the time integration of this dynamical system such as a second or third order Runge-Kutta methods, a linearized one-step implicit schemes or a Gear method ...

1.2 ZeBuLoN : software overview

ZeBuLoN is an advanced object FEA solver with many non-linear solution procedures for material oriented analysis ([1]). Originally developed as a research and teaching tool in the late 1980's (existing as a Fortran code), Zebulon is actively being developed (in C++) as part of a close partnership between NW Numerics, the Ecole Nationale Superieure des Mines de Paris, Center des Materiaux, Transvalor, ONERA and the INSA de Rouen.

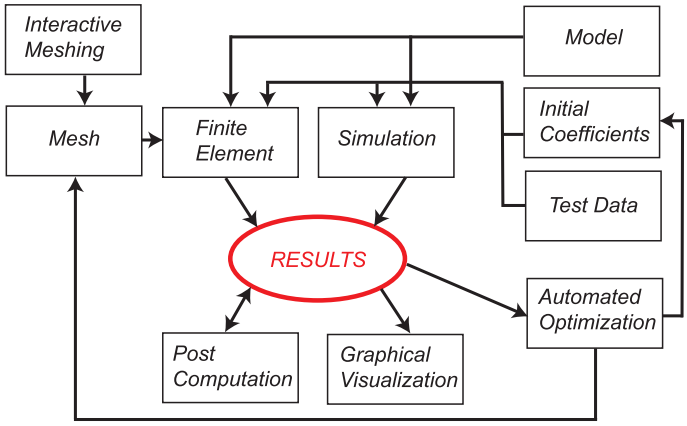

Figure 1: Interconnections possible between ZeBuLoN modules.

ZeBuLoN gives the user complete solution methods and provides a flexible environment in which to model materials behavior. The software package contains various modules (figure 1), from mesh creation (2D/3D), through advanced non-linear finite element calculation to flexible and accurate post processing, results visualization and presentation.

2. Mesh movement and deformation in the CEDRE code

The state of the fluid is characterized by a set of conserved quantities per unit volume $q(\mathbf{x}, t)$ (species densities, momentum, energy, turbulent quantities) governed by balance equations :

$$\partial_t q = -\nabla \cdot (\mathbf{v}\, q + \mathbf{f}), \tag{1}$$

where $\mathbf{v}$ denotes the fluid velocity $\mathbf{v} = \mathbf{v}(q)$ and the convective flux density $\mathbf{v}\ q$ has been split from other contributions $\mathbf{f} = \mathbf{f}(q, \nabla q, ...)$. Note that any uniform field q_0 is a steady solution of equation (1).

Let $V(t)$ be a time-dependant control volume bounded by a closed surface $A(t)$ with outward normal $\mathbf{n}(t)$ and local velocity $\mathbf{w}(\mathbf{x}, t)$. The integral form of (1) on $V(t)$ reads

$$\frac{d}{dt}\int_{V(t)} q\, dV = -\int_{A(t)} q(\mathbf{v}-\mathbf{w})\cdot\mathbf{n}\, dA - \int_{A(t)} \mathbf{f}\cdot\mathbf{n}\, dA. \tag{2}$$

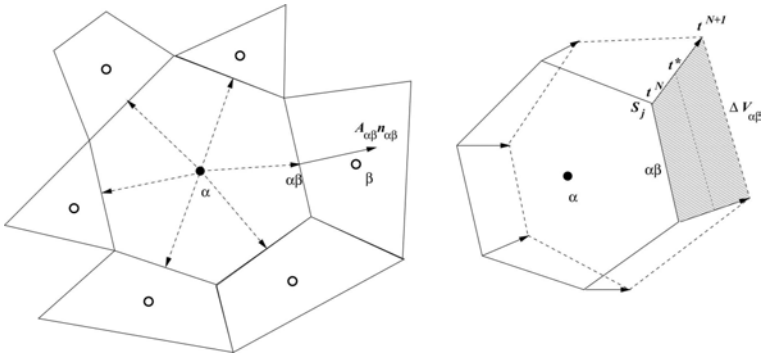

Figure 2: A cell and its neighbors, cell movement and deformation

In the particular case where q is uniform and constant, equation (2) reduces to

$$\frac{d}{dt}\int_{V(t)} dV = \int_{A(t)} \mathbf{w}\cdot\mathbf{n}\; dA, \tag{3}$$

which is the *volume conservation equation* kinematic identity. Therefore, any uniform field q_0 is a steady solution of (2) on $V(t)$. Figure (2) sketches a cell α and its neighborhood, in the two-dimensional case :

- The position $\mathbf{x}_j(t)$ and velocity $\mathbf{w}_j(t) = \dfrac{d\mathbf{x}_j}{dt}$ of each vertex S_j are known as time functions.
- The edges between vertices are straight lines. In the two-dimensional case, faces are edges. For a three-dimensional mesh, faces are triangulations build on contours made from edges, the common point of the triangulation being the gravity center of the face.

In all cases, the geometry and kinematics of each face (and each cell) is thus precisely known. Considering each cell as a closed volume, the integral outward normal vector is zero :

$$\sum_\beta \int_{A_{\alpha\beta}} \mathbf{n}\; dA = 0. \tag{4}$$

Let us define the area $A_{\alpha\beta}$ and the unit normal $\mathbf{n}_{\alpha\beta}$ by $A_{\alpha\beta}\mathbf{n}_{\alpha\beta} = \int_{A_{\alpha\beta}} \mathbf{n}\; dA$. Hence, equation (4) can be rewritten as :

$$\sum_\beta A_{\alpha\beta}\mathbf{n}_{\alpha\beta} = 0. \tag{5}$$

and each cell satisfies the volume conservation identity :

$$\frac{dV_\alpha}{dt} = \sum_\beta \int_{A_{\alpha\beta}} \mathbf{w}\cdot\mathbf{n}\; dA. \tag{6}$$

Let us define the mean normal face velocity $w_{n,\alpha\beta}$ by $A_{\alpha\beta}w_{n,\alpha\beta} = \int_{A_{\alpha\beta}} \mathbf{w}\cdot\mathbf{n}\; dA$. Then, equation (6) can be rewritten as :

$$\frac{dV_\alpha}{dt} = \sum_\beta A_{\alpha\beta}w_{n,\alpha\beta}. \tag{7}$$

In opposition to many ALE implementations, the volume conservation (7) is not explicitly added to the set of balance equations, but is a mere consequence of the unambiguous definition of geometry.

2.1 Space discretization

The exact balance equation (2) on cell α is

$$\frac{d}{dt}(V_\alpha q_\alpha) = -\sum_{\alpha\to\beta}\int_{A_{\alpha\beta}(t)} q(v_n - w_n)\, dA - \sum_{\alpha\to\beta}\int_{A_{\alpha\beta}(t)} f_n\, dA, \tag{8}$$

where

$$q_\alpha = \frac{1}{V_\alpha}\int_V q\, dV \tag{9}$$

is the mean cell value of q. Discretization approximates the flux integrals on the right hand side of (8). For a piecewise linear reconstruction, each integral is evaluated through a one-point quadrature at the face center $\alpha\beta$:

$$\frac{d}{dt}(V_\alpha q_\alpha) = -\sum_{\alpha\to\beta}\Big[q_{\alpha\beta}(v_{n,\alpha\beta} - w_{n,\alpha\beta}) + f_{n,\alpha\beta}\Big]A_{\alpha\beta} \tag{10}$$

In these approximate fluxes, $q_{\alpha\beta}$, $v_{n,\alpha\beta}$ et $f_{n,\alpha\beta}$ are evaluated through reconstruction techniques and numerical fluxes (see [10], [8] for instance). An important property of the discretization lies in the *consistency* of interface approximations : if $q_\alpha = q_0 = constant$ on the discretization stencil, one also has $q_{\alpha\beta} = q_0$, $\mathbf{v}_{\alpha\beta} = \mathbf{v}(q_0)$, $\mathbf{f}_{\alpha\beta} = \mathbf{f}(q_0)$. In this special case, equation 10 reads :

$$\frac{d}{dt}(V_\alpha q_\alpha) = -\sum_{\alpha\to\beta}\Big[q_0(v_{n,0} - w_{n,\alpha\beta}) + f_{n,0}\Big]A_{\alpha\beta}, \tag{11}$$

or

$$V_\alpha\frac{dq_\alpha}{dt} = -\sum_{\alpha\to\beta}\left[q_0 v_{n,0} + f_{n,0}\right]A_{\alpha\beta} + q_0(-\frac{dV_\alpha}{dt} + \sum_{\alpha\to\beta} w_{n,\alpha\beta}A_{\alpha\beta}). \tag{12}$$

On the right-hand side of equation 12, the first term is zero by considering equation 5 and the second also due to volume conservation (equation 7). Therefore, space discretization automatically satisfies uniform steady solutions for any mesh mouvement or deformation.

2.2 Time integration

Figure (2) shows the evolution of a cell during a time step $\Delta t = t^{N+1} - t^N$. Every vertex S_j moves between two known positions $\mathbf{x}_j^N$, $\mathbf{x}_j^{N+1}$ and the velocity is approximated by the constant vector $\frac{1}{\Delta t}(\mathbf{x}_j^{N+1} - \mathbf{x}_j^N)$. As previously indicated, these laws completely define the cell geometry during any time step. Note in particular that the volume $\Delta V_{\alpha\beta}$ swept by the face during the time step is exactly known.

The explicit Euler scheme for the semi-discrete balance, equation (11) reads

$$\frac{V_\alpha^{N+1}q_\alpha^{N+1} - V_\alpha^N q_\alpha^N}{\Delta t} = -\sum_{\alpha\to\beta}\Big[q_{\alpha\beta}^N(v_{n,\alpha\beta}^N - w_{n,\alpha\beta}^*) + f_{n,\alpha\beta}^N\Big]A_{\alpha\beta}^* \tag{13}$$

The area and face velocity on the right-hand side are relative to an intermediary state $*$ chosen to ensure exact volume conservation. More precisely, since $q_\alpha^N = q_\alpha^{N+1} = q_0$ must be a steady solution of (13), then we have :

$$\frac{V_\alpha^{N+1} - V_\alpha^N}{\Delta t} = \sum_\beta w_{n,\alpha\beta}^* A_{\alpha\beta}^*. \tag{14}$$

We can chose for instance $t^* = \frac{1}{2}(t^{N+1} + t^N)$, which gives a definite value for $A_{\alpha\beta}^*$. On the other hand, $V_\alpha^{N+1} - V_\alpha^N$ must be equal to the sum of volumes $\Delta V_{\alpha\beta}$ swept by the faces. Then, if we chose $w_{n,\alpha\beta}^* = \frac{\Delta V_{\alpha\beta}}{A_{\alpha\beta}^*\Delta t}$,

relation (14) will be automatically satisfied. As a consequence, we see that it is easy to satisfy volume conservation and respect uniform solutions through time integration.

Due to stability and precision, the explicit Euler scheme is never used in such form. However, this constitues a first step of all the explicit and implicit formulations and is thus a good illustration of the integration of mesh mouvement in all time-discretization schemes.

2.3 Generation of the mesh movement

In CEDRE, mesh movement and deformation can be generated either via user functions or propagation from boundaries through specific libraries. In the present study, an analytic law has been used considering the simple mesh-motions in all the studied cases. This analytic law use a propagation radius R, a damping coefficient α and an exponential coefficient b such as :

$$\begin{aligned} \text{if } r > R \text{ then } \alpha = 0, \\ \text{if } 0 < r < R \text{ then } \alpha = a^b, \end{aligned} \tag{15}$$

where r is the distance from the closest coupled boundary and $a = 1 - \frac{r}{R}$. Node displacement are then updated and displacement x is defined by

$$x(t + \Delta t) = x(t) + \alpha \times x_p, \tag{16}$$

where x_p is the closest coupled node displacement.

3. COUPLING PROCEDURE

In the coupled approach used, the FSI is achieved by partitioning the problem into fluid and solid parts solved separately with boundary conditions calculated by the other part. In this partitioned procedure, the coupled problem is numerically solved using a Conventional Serial Staggered approach ([11]).

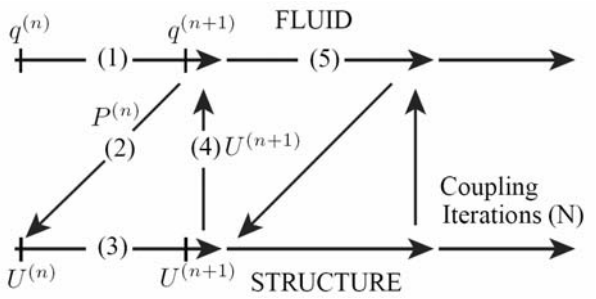

Figure 3: FSI numerical procedure.

Figure 3 shows the sequence of iteration steps. It starts with the calculation of the aerodynamic field (path 1). The resulting pressure distribution P is transferred to the finite element nodes (path 2). Using this new interface conditions the structural code computes the deformation U of the structure (path 3). The resulting displacements modify the fluid surface grid and consequently change the boundary conditions (path 4) but also the entire grid in the fluid domain in the next step (path 5). Note that, in all the following FSI computations, matching grids between fluid and solid are employed and therefore no non-matching load transfer scheme need to be used in this study

4. VALIDATION SIMULATIONS

This section discusses several verification and validation simulations performed in order to assess the precision of the code coupling herein described. Two transient test problems involving an inviscid fluid coupled with a solid are investigated. The interface between the two domains is assumed to be impermeable, non-reactive and adiabatic and thus can be treated as a contact discontinuity.

4.1 One-Dimensional problem

The first test simulation is a quasi-1D problem and has an analytical solution, [9], for the case of an inviscid compressible flow interacting with a linearly elastic solid. This problem involves the analysis of a transient FSI consisting of expansion fans in the fluid domain coupled with a compression wave in elastic material domain.

Initially, the system is at rest. The solid is unstressed and uniform conditions are applied to the fluid domain (figure 4). At time $t = 0$, uniform pressure stress is applied to the solid resulting in the motion of the interface at a constant velocity u_i. This problem can be seen as a flexible piston problem with expansion fans propagating in the fluid domain and a compression wave in the elastic domain.

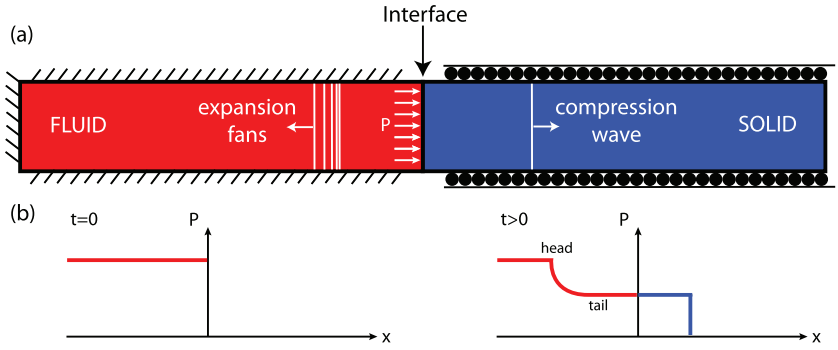

Figure 4: (a) Scheme of the elastic piston problem and (b) pressure as a function of x for simple centered expansion fans in fluid domain and compression wave in solid domain.

At the interface ($x = 0$) of the two domains, no mass flux, no jump in normal velocity and normal stress are allowed. Furthermore, a free-slip boundary condition for the tangential velocity and no end-reflection wave are considered

4.1.1 Analytical Solution

An expansion wave is produced in the fluid domain by the motion of the flexible solid interface. Such left-running wave is defined as a simple wave and has straight C_- characteristics $x = (u - a)t$ along which the flow properties are constant. Moreover, because the wave originates from the interface point $(x, t) = (0, 0)$, it is called a centered expansion wave.

Considering an isentropic process and applying the method of characteristics, the Riemann invariant for a calorically perfect gas is carried through the expansion wave. Hence :

$$u + \frac{2a}{\gamma - 1} = \text{const through the wave,} \tag{17}$$

where p denotes pressure, u and a the local values of mass velocity and speed of sound, respectively. By applying equation 17 in the fluid region :

$$u(x,t) + \frac{2c(x,t)}{\gamma - 1} = 0 + \frac{2c_o}{\gamma - 1} = u_i + \frac{2c_i}{\gamma - 1}, \tag{18}$$

where o and i subscripts denotes respectively the initial state of fluid and the interface values.

Also because the flow is isentropic, $p_i/p_0 = (\rho_i/\rho_0)^\gamma$, where ρ denotes density. Therefore, equation 18 yields :

$$\frac{p_i}{p_0} = \left[1 - \frac{\gamma - 1}{2}\left(\frac{u_i}{c_0}\right)\right]^{\frac{2}{\gamma-1}} \tag{19}$$

and gives the properties in a simple expansion wave as a function of the local gas velocity in the wave. Considering an isentropic, linear elastic material occupying the right side of the interface. For $t > 0$, from Navier's equation we have the one-dimensional wave propagation equation of an elastic longitudinal wave (P-wave) under plane stress assumption :

$$\frac{\partial^2 \xi}{\partial x^2} = \frac{1}{{c_d}^2}\frac{\partial^2 \xi}{\partial t^2}, \tag{20}$$

where ξ is the displacement field, $c_d = \sqrt{\frac{E}{\rho_s(1-\nu^2)}}$ the longitudinal wave speed of the solid, E the Young's modulus, ν the Poisson's ratio and ρ_s the solid density. Considering a uniform pressure σ_i applied to the interface, we obtain :

$$|\sigma_i| = \rho_s c_d \dot{\xi}_i. \tag{21}$$

The coupled system (equations 19 and 21) can be solved by the use of a Newton method and imposing kinematic continuity ($u_i = \dot{\xi}_i$) and mechanical equilibrium ($\sigma_i = p_i$) at the interface.

4.1.2 Numerical Solution

The gas is assumed to be ideal air ($\gamma = 1.4$) at $T = 300°\mathrm{K}$ with an initial pressure $p_o = 101325\,\mathrm{Pa}$. The elastic solid is an artificial material with Poisson's ration $\nu = 0.29$, density $\rho_s = 2800\,\mathrm{kg.m^{-3}}$ and Young's modulus $\mathrm{E} = 1.0 \times 10^7$ Pa. From these properties, the speed of sound in the fluid is $a = 347\,\mathrm{m.s^{-1}}$ and longitudinal wave speed $c_d = 62.45\,\mathrm{m.s^{-1}}$ in the solid under plane stress assumption. The coupled system yields to to an analytical interface velocity $u_i = 0.578\,\mathrm{m.s^{-1}}$.

In this partitioned procedure, the coupled problem is numerically solved using a coupling period $\mathrm{T_{coupling}} = 1 \times 10^{-6}\,\mathrm{s}$ equal to the fluid and solid solvers time steps.

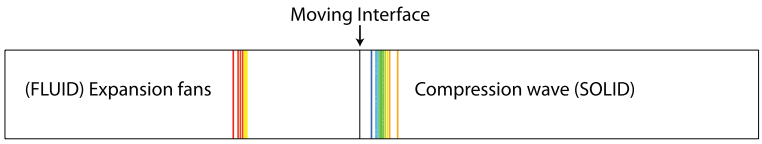

Figure 5: Pressure and stress contour plot.

Figure 5 shows the wave motion for expansion wave in the fluid domain and a compression wave propagating in the solid domain. Contour plots of the stress and pressure distribution numerically obtained fairly agree with the assumption of one-dimensionality. Furthermore, several computations had been carried out for different matching-meshes densities and lead to the same conclusions.

Figure 6-(a) depicts the comparison between the numerical interface displacement and the one-dimensional analytical solution for the first millisecond. The interface velocity resulting from the code coupling is consistent with the uniform speed theoretically predicted but presents some oscillatory errors (figure 6-(b)). Nevertheless, this error tends to reach a value less than 10^{-2} and probably indicates that the coupling algorithm could be optimized.

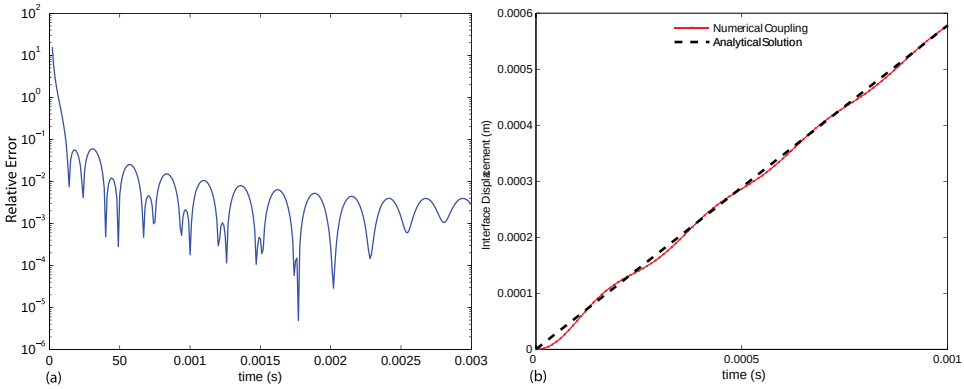

Figure 6: Numerical and analytical interface displacement, (a) Relative error and (b) Interface displacement as a function of time.

4.2 Two-Dimensional problem

In order to assess the potentiality of the coupling strategy in handling two-dimensional transient FSI problems, an experimental case, performed by the IUSTI laboratory ([7]) has been computed. Such experimental device describes a flexible panel protruding into a shock tube and submitted to a shock wave. A close-up view of the experimental set-up is given in figure 7

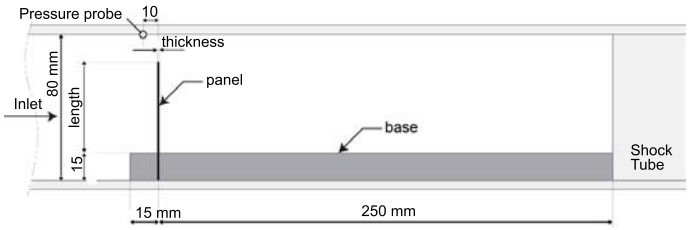

Figure 7: IUSTI experimental setup.

The panel is fixed in a base assumed infinitely rigid. As the shock travels down the tube, pressure gradients results in a panel motion. In this experiment, fluid pressure evolution is measured by a pressure transducer and top panel displacement monitored. Furthermore, ombroscopic pictures provide visual information on the behavior of the transmitted and reflected shocks.

4.2.1 Numerical model

The coupled simulation is performed considering an isotropic steel panel (linear elastic with a Young's Modulus $E = 220\,\text{GPa}$ and a density $\rho = 7600\,\text{kg}$) with a length equal to 40 mm and 1 mm thickness. The shock wave moves from the inlet boundary condition, where air is injected at standard atmosphere conditions (1.0×10^5 Pa and $T = 293°\text{K}$), at a Mach number of 1.2. Considering the short duration of the experimental run, turbulence is neglected. For such compressible flow, Rankine-Hugoniot relations allow determination of pressure and temperature values dealing with the shock wave. The entire calculation fluid domain is approximately composed of 45000 cells and has a characteristic cell dimension about 1 mm in the region close to the deformable panel. The coupling time step is taken to be equal to 10^{-6} s which is about 100 times smaller than the structure characteristic time. Considering the mesh resolution and time step, one can states that numerical parameters can assure sufficient precision of the coupled dynamic.

4.2.2 Numerical results and comparison to experimental data

Interaction between shockwave and panel gives rise to a transmitted and reflected shockwave. A detailed description of the physical phenomena involved is discussed in details by J. Giordano and can be found in [7]. As the figure 8 shows, numerical schlierens compared to experimental ombroscopic pictures present a good agreement and thus indicates that the flow field dynamic is quite well captured.

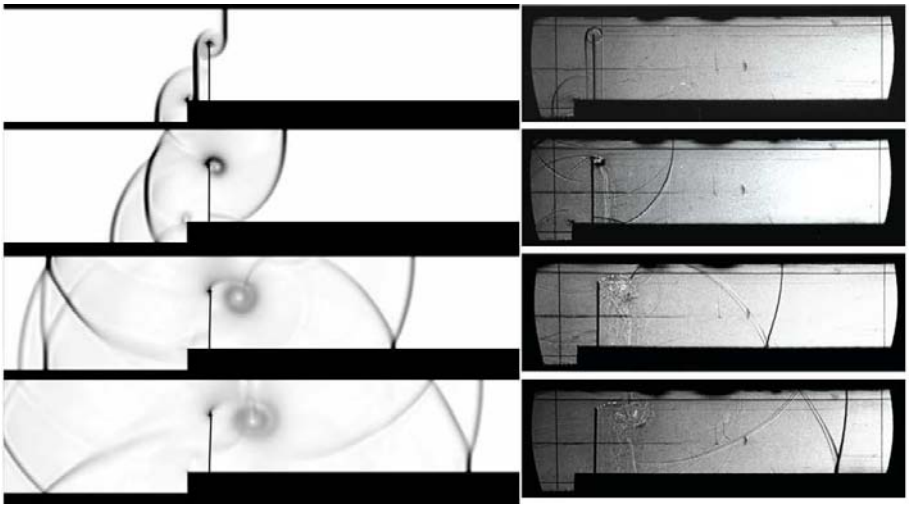

Figure 8: Numerical schlierens (left) and experimental ombroscopic pictures (right).

Paying particular attention on the pressure time evolution, a plot of the pressure at the position of the experimental transducer is reported on figure 9. Although a slight difference exists for $t > 0.0025$ s, probably due to some boundary condition reflection error for the reflected shockwave, the two plots exhibit a similar transient evolution. As a result from fluid dynamic loads, the panel movement, figure 9, is also well captured and falls within experimental uncertainties.

All these comparisons between numerical and experimental data emphasize that the coupling methodology succeed when computing highly transient phenomena and thus should be used to cope with more elaborate computations involving stronger coupling phenomena.

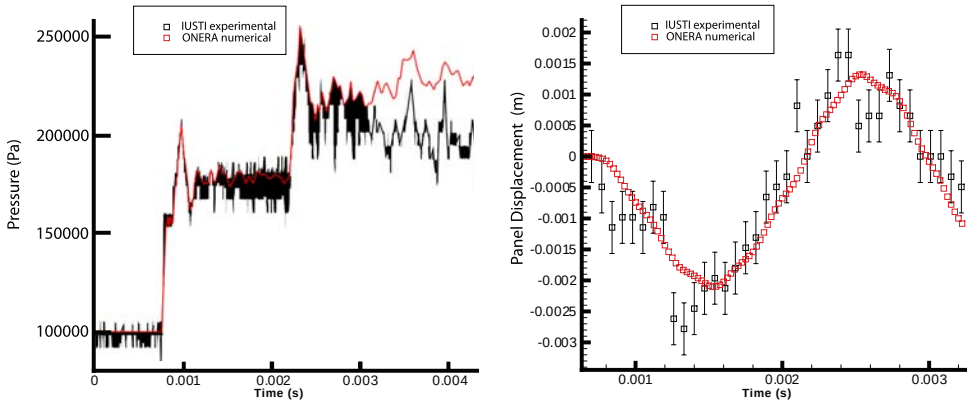

Figure 9: Pressure time evolution at probe location (left) and corresponding panel tip deflection (right).

5. APPLICATION TO THE FIELD OF SOLID ROCKET PROPULSION

Fluid Structure Interaction (FSI) in SPRM is a complex phenomenon involving aeroacoustics interacting with the non-linear mechanical behavior of the inhibitor. Within the framework of pressure oscillations investigation ([13]), a quasi-static case is computed in order to validate the partitioned coupling methodology. The studied geometry is a simplified small scale configuration of the Ariane 5 SPRM allowing precise determination of the inhibitor deflection ([5]).

5.1 VALDO setup

The experimental facility VALDO (sketched in figure 10) is a modular axisymmetric cold flow setup similar to the device imagined by Brown and co-workers ([4]). A detailed description of the setup may be found in [2]. The experimental setup is composed of injecting modules equipped, in their central part, with porous tubes. The injection velocity is assumed to be normal to the wall and with a constant norm in space. Among the injecting modules, one measurement module monitors pressure, temperature and velocity inside the chamber.

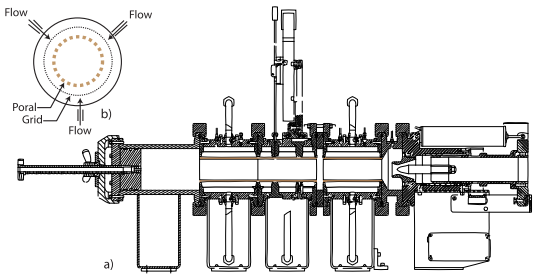

Figure 10: Scheme of the VALDO setup. a) general view, b) sketch of an injecting element.

The similarity with full scale motors is based on the conservation of the Mach number but the Reynolds[1] number range is one order of magnitude smaller. A non-intrusive measurement system using a laser interferometer ([5]), allowing both displacement and frequency measurements of flexible inhibitors, has been chosen in order to measure the inhibitor response under fluid stresses.

5.2 FSI experimental Static Reference Case

One of the main objectives of this experimental test is to provide data aiming at validating the coupled computations. The VALDO set-up has been used in a configuration representative of SPRM. The geometry is composed of three injecting modules, a non injecting intersegment and an aft end cavity with submerged nozzle. A $2\,mm$ thick inhibitor of elastomeric material is clamped between the intersegment cavity and the third injecting module. Parametric details are given in figure 11.

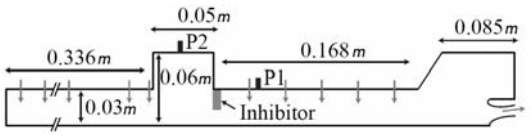

Figure 11: VALDO configuration used for Static Reference Case

[1]Reynolds number is expressed as function of the injected mass flow rate and inner radius

The non intrusive measurement system provides measurement of inhibitor's vibration velocity measurement. Displacements (shown in figure 12) are then computed by integrating the velocity vibration over time. Air is injected at $1.19\,\mathrm{m.s^{-1}}$ inside the chamber and structure deflection due to fluid stress loading is monitored.

Under fluid stress loading, for an internal pressure chamber of about 2 bar, a disparity in pressure on each side of the inhibitor creates a bending moment. As a consequence, the inhibitor bends and reaches a quasi-steady state with a maximum deflection $d_{max} = 3.285\,\mathrm{mm}$ on its top. Such experimental data provides values of deflection that can be used for coupled simulation validation.

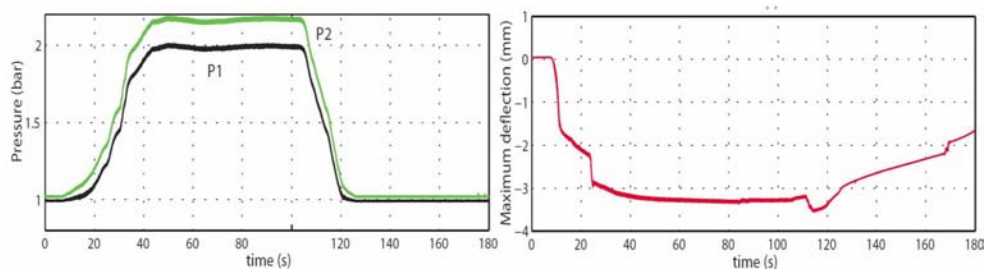

Figure 12: Pressure evolution (left) and maximum deflection of the inhibitor (right).

5.3 Numerical Results

The coupling algorithm for this coupled computation is the same used, few years ago by Roach and al. ([12]). It assumes steady state approach for the aerodynamic field calculation (figure 3-path 1). Once the fluid has reached a steady state the pressure distribution is transferred to the structure in order to compute the resulting deformations.

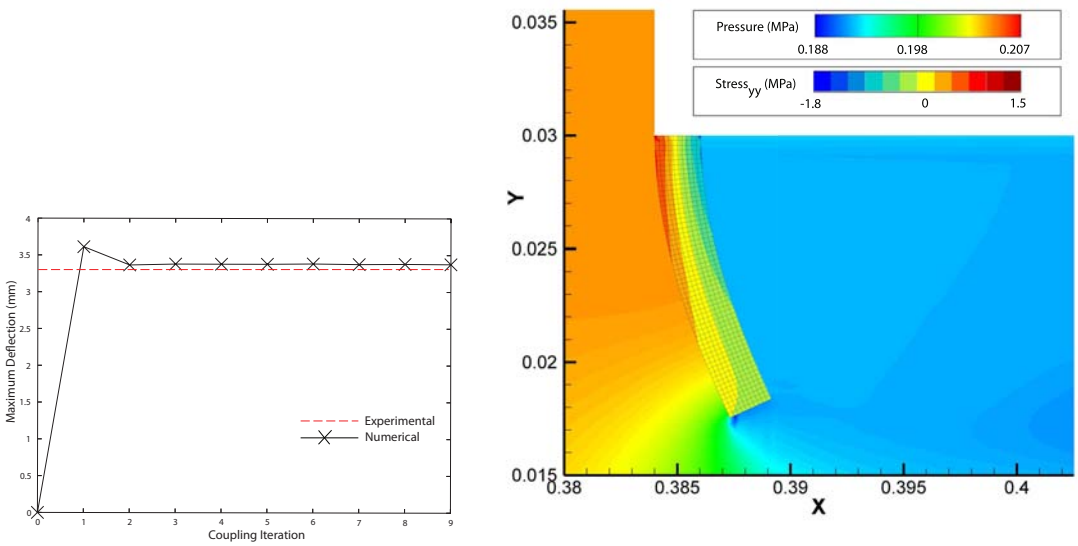

Figure 13: Maximum deflection of the inhibitor as a function of number of coupling iterations (Left). Mean pressure field and principal stress of the inhibitor (Right).

After ten coupling iterations the inhibitor's deflection seems to have reached a quasi-static value. Its maximum deflection against coupling iteration is plotted in figure 13. More precisely, the quasi-steady

deflection is quickly approached after 3 coupling iterations and presents a good agreement with experiment. However, one can note that a slight difference is observed between experimental and numerical value and thus indicates that inhibitor's rheological parameters could be optimized.

From this computation, one can state that the coupling method provides good prediction of the inhibitor deflection under fluid pressure and therefore constitues an efficient solution for studying FSI inside SPRM.

6. CONCLUSION

In this paper we have addressed the development and validation of the ONERA coupling procedure between fluid and solid solvers, namely CEDRE and ZeBuLoN. A number of verification simulations has been described and demonstrate the accuracy of the coupling methodology when computing static and highly transient FSI problems.

As a first step to FSI investigation inside SPRM, a small scale configuration has been computed. With the aid of experimental data, the coupling methodology has been shown to be adequate when studying the quasi static deflection of an inhibitor under fluid loads. According to Flandro's work, [6],vortex shedding from inhibitors has been identified as a possible mechanism for the excitation of the acoustic modes of a combustion chamber. Future work will pursue numerical investigation of pressure oscillations inside SPRM by taken into account the dynamic response of inhibitors in such simplified configuration.

7. ACKNOWLEDGEMENTS

This study has been supported by the French Space Agency CNES and by ONERA. Authors wish to gratefully acknowledge N. Cesco and E. Robert, from the CNES Launcher Directorate, for their encouragement. They also thank G. Avalon and D. Lambert from ONERA for the realization of VALDO experimental tests.

References

[1] Z-set, finite element solver and material constitutive model library. *http://www.nwnumerics.com/.*

[2] G. Avalon and T. Josset. Cold gas experiments applied to the understanding of aeroacoustic phenomena inside solid propellant boosters. *42nd AIAA/ASME/SAE/ASEE Joint Propulsion Conference and Exhibit, AIAA Paper 2006-5111*, July 2006.

[3] N. Bertier, B. Courbet, D. Dutoya, F. Vuillot, and P. Sagaut. Large eddy simulation of a subsonic flow over a cavity on general unstructured grids. *AIAA paper 2004-0679*.

[4] R.S. Brown, R. Dunlap, S.W. Young, and R.C. Waugh. Vortex shedding as an additional source of acosutic energy in segmented solid propellant rocket motor. *Journal of Spacecraft and Rocket*, 18:312–319, 1981.

[5] S. Cerqueira, F. Feyel, and G. Avalon. A first step to fluid-structure interaction inside solid propellant rocket motors. *Proceedings of Fluid Structure Interaction V*, 2009.

[6] G. A. Flandro. Vortex driving mechanism in osillatory rocket flows. *Journal of Propulsion and Power*, 2(3):206–214, 1986.

[7] J. Giordano and al. Shock wave impacts on deforming panel, an application of fluid-structure interaction. *Shock Waves*, 14:103–110, 2005.

[8] F. Haider, J.-P. Croisille, and B. Courbet. Stability analysis of the cell centered finite-volume muscl method on unstructured grids. *Numerische Mathematik (In press)*, 2009.

[9] R.K. Jaiman, X. Jiao, P.H. Geubelle, and E. Loth. Assessment of conservative load transfer for fluid-solid interface with non-matching meshes. *International Journal for numerical methods in engineering*, 64:2014–2038, 2005.

[10] Chevalier P. and al. Cedre: development and validation of a multiphysic computational software. *1st European Conference for Aerospace Sciences (EUCASS)*, 2005.

[11] S. Piperno, C. Farhat, and B. Larrouturou. Partitioned procedures for the transient solution of coupled aroelastic problems part i: Model problem, theory and two-dimensional application. *Computer Methods in Applied Mechanics and Engineering*, 124:79–112, 1995.

[12] R.L. Roach, K. Gramoll, M. Weaver, and G.A. Flandro. Fluid-structure interaction of solid rocket motor inhibitors. *AIAA, SAE, ASME, and ASEE, 28th Joint Propulsion Conference and Exhibit, Nashville, TN*, July 1992.

[13] S. Scippa, P. Pascal, and F. Zanier. Ariane 5-mps - chamber pressure oscillations full scale firing results: Analysis and further studies. *AIAA Paper 94-3068*, June 1994.